Modeling the spectral conductivity of Al-Mn-Si quasicrystalline approximants: A phenomenological approach

Enrique Maciá
Departamento Física de Materiales, Facultad CC. Físicas, Universidad Complutense de Madrid, E-28040 Madrid, Spain

Tsunehiro Takeuchi and Toshio Otagiri
Department of Crystalline Materials Science, Nagoya University, Nagoya 464-8603, Japan
(Received 10 June 2005; revised manuscript received 12 September 2005; published 28 November 2005)

The electronic structure of a quasicrystalline approximant sample is analyzed by means of a combined study of different experimental transport curves within a phenomenological approach. The main features of the obtained spectral conductivity are discussed and compared to those corresponding to icosahedral quasicrystals. Such a comparison provides interesting clues about the role of quasiperiodic order and of local atomic arrangements in the origin of unusual behaviors in the electrical conductivity and thermopower observed in complex metallic alloys.

DOI: 10.1103/PhysRevB.72.174208 PACS number(s): 61.44.Br, 71.20.−b, 72.15.−v, 72.15.Jf

I. INTRODUCTION

Following the discovery of thermodynamically stable quasicrystalline alloys of high structural quality,[1] a lot of detailed experimental studies have confirmed the existence of quite unusual transport properties in quasicrystals (QCs).[2–4] In this way, it has been progressively realized that the temperature dependence of electrical conductivity, Hall and Seebeck coefficients, and thermal conductivity, resemble a more semiconductorlike than metallic character.[5–7]

By the light of these experimental results the fundamental question arises concerning whether these transport anomalies should be mainly attributed (or not) to the characteristic quasiperiodic order of QCs structure. In this regard, experimental evidence showing that the structural evolution from the amorphous to the quasicrystalline state is accompanied by a parallel evolution of the electronic transport anomalies[8] clearly indicates the importance of short-range effects on the emergence of some transport anomalies. In fact, broadly speaking one should expect that the nature of the chemical bonding determining the local atomic arrangements would play a significant role in most physical properties of these materials.[9–11] Accordingly, crystalline approximants (ACs), which exhibit a local atomic environment very similar to their related QC alloys, appear as natural candidates to investigate the relative importance of short-range versus long-range order effects on the transport properties.

On the basis of detailed *ab initio* band structure calculations Landauro and Solbrig proposed a spectral conductivity model $\sigma(E)$ satisfactorily describing the transport properties of both QCs and ACs in a wide temperature range.[12–14] Making use of this electronic structure model a phenomenological approach relating several topological features (such as maxima, minima, or sign reversals) in the transport coefficients temperature dependence to certain features in the electronic structure of the samples was subsequently introduced.[15–19] In so doing, analytical expressions describing the main topological features of the electrical conductivity, $\sigma(T)$, and thermoelectric power, $S(T)$, curves were derived in terms of a set of phenomenological coefficients, ξ_j, and compared to the experimental curves reported for a number of quasicrystalline samples.[17–19]

In this work we shall extend the applicability of our phenomenological approach in order to extract useful information about the electronic structure of ACs. As a suitable sample we consider the $Al_{82.6-x}Mn_{17.4}Si_x(x=9)$ alpha phase,[20] which is a well-documented representative of the 1/1-cubic approximants class. This AC exhibits a sign reversal in the thermoelectric power with increasing temperature,[20] (a feature which cannot be accounted for in terms of the usually employed Mott formula), in close analogy with the behavior observed in some high quality QCs. The main goal of this work is to gain some insight into the physical effects intrinsically related to local order effects as compared to those related to the characteristic quasiperiodic order of QCs. To this end, we first determine the phenomenological coefficients values from a combined fitting analysis of different experimental transport curves. Then we derive the AC's spectral conductivity function and compare it with that corresponding to previously studied QCs. From this comparison interesting clues about the role of fine spectral features related to the local atomic arrangement are obtained.

The paper is organized as follows. In Sec. II we describe the experimental procedure. In Sec. III, we present the obtained transport curves and analyze them in terms of the analytical expressions previously derived within the context of our phenomenological approach. Section IV is devoted to a discussion of the physical implications of the obtained phenomenological coefficients values. In Sec. V we explicitly derive the electronic structure model parameters and discuss the reliability of the obtained $\sigma(E)$ function on the basis of specific heat measurements. Finally, in Sec. VI we summarize the main conclusions of this work.

II. EXPERIMENTAL PROCEDURE

Mother ingots of $Al_{73.6}Mn_{17.4}Si_9$ were prepared by the induction-melting method under a pressurized Ar atmo-

 ©2005 The American Physical Society

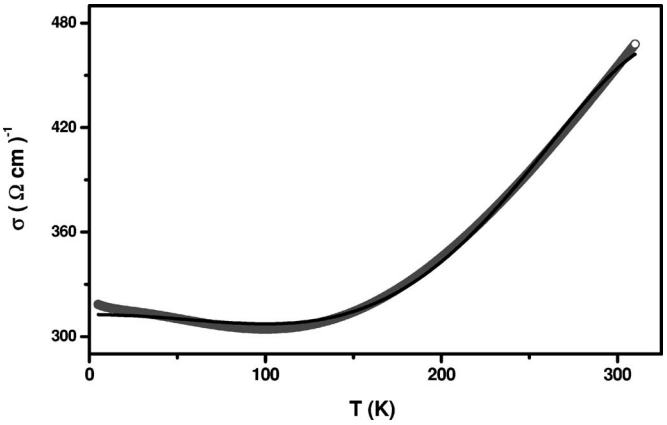

FIG. 1. Electrical conductivity as a function of temperature for the $Al_{73.6}Mn_{17.4}Si_9$ cubic approximant (open circles). The solid line corresponds to the best fit curve $\sigma(T)=\sigma_0(1+BT^2+CT^4+DT^6)$ with $\sigma_0=312.6\pm0.2\ (\Omega\,\mathrm{cm})^{-1}$, $B=(-3.50\pm0.08)\times10^{-6}\ \mathrm{K}^{-2}$, $C=(1.91\pm0.02)\times10^{-10}\ \mathrm{K}^{-4}$, $D=(-1.07\pm0.02)\times10^{-15}\ \mathrm{K}^{-6}$, with a correlation coefficient $r=0.9824$.

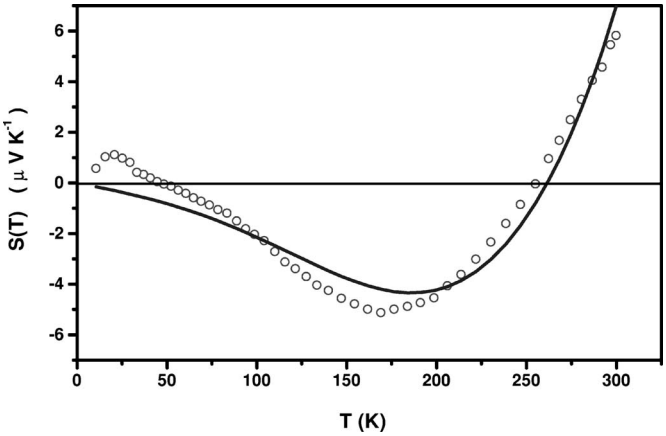

FIG. 2. Thermoelectric power as a function of temperature for $Al_{73.6}Mn_{17.4}Si_9$ cubic approximant (open circles). The solid line corresponds to the best fit curve given by Eq. (6) with $a=0.29\pm0.05\ (\mathrm{eV})^{-1}$, $f=(6\pm2)\times10^{-5}\ \mathrm{K}^{-2}$, and $g=(-1.1\pm0.3)\times10^{-9}\ \mathrm{K}^{-4}$, with Pearson $\chi^2=0.562$.

sphere. Some of the mother ingots were melted again and rapidly quenched on a copper wheel of 200 mm in diameter rotating at 3000 rpm. Quenched ribbons and the bulk ingots were annealed at 700 C° for 24 h. X-ray diffraction (XRD) peaks of the annealed samples were successfully identified as those corresponding to the 1/1-cubic approximant, with no secondary phases.[20]

Electrical conductivity $\sigma(T)$ was measured in a temperature interval ranging from 2 to 300 K with the Physical Properties Measurement System, Quantum Design Inc. (QD-PPMS), Seebeck Coefficient Measurement System of MMR Technologies Inc. (MMR-SCMS), and the thermal-transport option (TTO) of the QD-PPMS were employed for the thermoelectric power measurements within the temperature ranges of $90\leqslant T\leqslant400$ K and $10\leqslant T\leqslant300$ K, respectively. The ribbon samples were used for the measurements of $\sigma(T)$ and $S(T)$ with the MMR-SCMS, and the bulk samples for the measurements of $S(T)$ with the QD-PPMS-TTO.

$Al_{82.6-x}Mn_{17.4}Si_x(x=7,8,10,11,12)$ 1/1-cubic approximants without any precipitation of secondary phases were also prepared to measure the Si concentration dependence of the electronic specific heat coefficient.[20] Low temperature specific heat measurement was performed using the relaxation method with the MLHC9H of Oxford Instruments in the temperature range from 0.5 to 10 K under a magnetic field up to 9 T. The magnetic field weakened the unfavorable effects of the Schottky-type anomaly from magnetic impurities as it was reported for the AlReSi cubic approximants.[21]

In Fig. 1 we show the temperature dependence of the electrical conductivity for the $Al_{73.6}Mn_{17.4}Si_9$ cubic approximant. The curve exhibits a typical metallic behavior up to ~100 K, where the conductivity attains a minimum and then progressively increases as the temperature is further increased. The $\sigma(T)$ curves of several QCs also exhibit a similar behavior in the low temperature regime. Thus, *i*-AlPdMn samples show a conductivity minimum located at about 40–60 K.[22] A less pronounced minimum is reached at lower temperatures (10–20 K) in the case of some *i*-AlCuFe samples.[6,23,24]

In Fig. 2 we show the temperature dependence of the thermoelectric power for the same approximant phase. The thermopower shows a remarkable nonlinear behavior, exhibiting a broad minimum at about $T_1=160$ K, and changes its sign twice at about $T_0=50$ K and 260 K, respectively. This anomalous behavior resembles that observed for several icosahedral QCs belonging to the *i*-AlCu(Fe,Ru) family.[24–29]

III. ANALYSIS OF THE TRANSPORT CURVES

In the temperature interval ranging from about 20–300 K approximately,[30] the electrical conductivity and thermopower curves can be well approximated by the expressions[16–18]

$$\sigma(T)=\sigma_0(1+\xi_2bT^2+\xi_4b^2T^4+(g_1\xi_4-g_2\xi_3)b^3T^6), \quad (1)$$

and

$$S(T)=-2|e|\mathcal{L}_0T\frac{\xi_1+\xi_3bT^2+\left(\frac{q_0}{4}g_2\xi_4-g_3\xi_3\right)b^2T^4}{1+\xi_2bT^2+\xi_4b^2T^4+(g_1\xi_4-g_2\xi_3)b^3T^6}, \quad (2)$$

respectively, where σ_0 is the residual electrical conductivity, $\mathcal{L}_0=\pi^2k_B^2/3e^2=2.44\times10^{-8}\mathrm{V}^2\,\mathrm{K}^{-2}$ is the Lorenz number, and $b\equiv e^2\mathcal{L}_0$. The set of parameters g_i and ξ_j can be explicitly expressed in terms of the electronic model parameters[16] (see the Appendix) and can be regarded as phenomenological coefficients containing detailed information about the electronic structure of the sample. Some phenomenological coefficients can also be related to the topology of the spectral conductivity function $\sigma(E)$ by means of the following expressions:[17]

$$\left(\frac{d\ln\sigma(E)}{dE}\right)_{E_F}=2\xi_1, \quad (3)$$

and

TABLE I. Phenomenological coefficients values for the $Al_{73.6}Mn_{17.4}Si_9$ cubic approximant as derived from a combined analysis of the experimental transport curves $\sigma(T)$ and $S(T)$.

Phenomenological coefficients
$\sigma_0 = 312.6 \pm 0.2\ (\Omega\ \mathrm{cm})^{-1}$
$\xi_1 = +0.29 \pm 0.05\ (\mathrm{eV})^{-1}$
$\xi_2 = -144 \pm 3\ (\mathrm{eV})^{-2}$
$\xi_3 = (+2.5 \pm 0.8) \times 10^3\ (\mathrm{eV})^{-3}$
$\xi_4 = (+3.21 \pm 0.03) \times 10^5\ (\mathrm{eV})^{-4}$

$$\left(\frac{d^2 \ln \sigma(E)}{dE^2}\right)_{E_F} = 2(\xi_2 - 2\xi_1^2), \tag{4}$$

where E_F is the Fermi level. Generally speaking the conductivity spectrum takes into account both the DOS structure, $N(E)$, and the diffusivity of the electronic states, $D(E)$, according to the Einstein's relationship $\sigma(E) = e^2 N(E) D(E)$. Thus, from the knowledge of the phenomenological coefficients ξ_1 and ξ_2 we can obtain suitable information concerning the slope and curvature of the DOS close to E_F.

In order to determine the values of the different phenomenological coefficients we proceed as follows. In the first place, we will fit the experimental $\sigma(T)$ curve shown in Fig. 1 to the trial function

$$\sigma(T) = \sigma_0(1 + BT^2 + CT^4 + DT^6), \tag{5}$$

where, according to Eq. (1), we have $B \equiv \xi_2 b$, $C \equiv \xi_4 b^2$, and $D \equiv (g_1 \xi_4 - g_2 \xi_3) b^3$. The fitting analysis results are given in the caption of Fig. 1. From the reported values we obtain $\xi_2 = B/b = -144 \pm 3\ (\mathrm{eV})^{-2}$ and $\xi_4 = C/b^2 = (3.21 \pm 0.03) \times 10^5\ (\mathrm{eV})^{-4}$, respectively. In order to obtain the remaining phenomenological coefficients we will fit the experimental $S(T)$ curve to the trial function (expressed in $\mu \mathrm{V\ K}^{-1}$)

$$S(T) = -0.0488T \frac{a + fT^2 + gT^4}{1 + BT^2 + CT^4 + DT^6}, \tag{6}$$

where, according to Eq. (2), we have $a \equiv \xi_1$, $f \equiv \xi_3 b$, $g \equiv (q_0 g_2 \xi_4 / 4 - g_3 \xi_3) b^2$, and we make explicit use of the fitting parameters B, C, and D previously obtained from the study of the electrical conductivity curve. In this way, the consistency between the phenomenological coefficients values derived from both transport curves is guaranteed. The fitting analysis results are given in the caption of Fig. 2. From the reported values we obtain $a = \xi_1 = 0.29 \pm 0.05\ (\mathrm{eV})^{-1}$, and $\xi_3 = f/b = (2.5 \pm 0.8) \times 10^3\ (\mathrm{eV})^{-3}$. In Table I we summarize the obtained values for the different phenomenological coefficients.

At this point, some words are in order regarding the possible contribution of phonon-drag effects on the thermopower curve shown in Fig. 2. Broadly speaking, one expects the phonon-drag contribution to play a major role in the intermediate temperature range, when a significant number of inelastic scattering events take place between phonons and electrons. At low temperatures the number of phonons able to efficiently interact is quite reduced and electrons are mainly elastically scattered by impurities and/or lattice defects. At high temperatures phonons are predominantly scattered among themselves and any significant interaction between electrons and phonons has little effect in the electrical transport properties. This physical scenario accounts well for the $S(T)$ peak occurring at less than 130 K in pure elements.[31] In the case of QCs, the absence of a well-defined lower limit for momentum transfer via quasiumklapp processes along with the complex structure of the Fermi surface make it difficult to estimate the relative contribution of the phonon-drag term in the overall thermopower.[32,33] On the basis of a detailed study on both the temperature and composition dependence of AlReSi ACs,[34] we expect a small phonon-drag contribution in the approximants case, where a natural scale for efficient umklapp processes is given by the reciprocal lattice. Accordingly, in the present work we do not consider phonon-drag refinements in the thermopower curve analysis.

IV. DISCUSSION

In Table II we compare the values of the phenomenological coefficients listed in Table I with those derived in previous works for different QCs belonging to the AlCu(Fe,Ru) and AlPdMn families.[17,18] As we can see the values for ξ_1 and ξ_2 coefficients are about one order of magnitude smaller for the approximant as compared to those corresponding to icosahedral QCs; meanwhile, the coefficients ξ_3 and ξ_4 take on comparable values for both the approximant and icosahedral QCs. In addition, the approximant's phenomenological coefficients ξ_2 and ξ_4 change their sign as compared to those obtained in the case of QCs.

TABLE II. Comparison among the phenomenological coefficients values of the $Al_{73.6}Mn_{17.4}Si_9$ cubic approximant and several icosahedral QCs. The data listed for the *i*-AlCu(Fe,Ru) QCs are mean values from three different samples (cf. Refs. 17 and 18).

Sample	$\xi_1\ (\mathrm{eV})^{-1}$	$\xi_2 \times 10^3\ (\mathrm{eV})^{-2}$	$\xi_3 \times 10^3\ (\mathrm{eV})^{-3}$	$\xi_4 \times 10^5\ (\mathrm{eV})^{-4}$
$Al_{73.6}Mn_{17.4}Si_9$	+0.3	−0.14	+2.5	+3.2
i-$Al_{64.5}Cu_{20}Ru_{15}Si_{0.5}$	+1.5	—	−1.5	—
i-AlCuFe	+5.6	+0.8	−1.7	−2.9
i-AlCuRu	+5.2	+1.5	−4.6	−6
i-$Al_{70}Pd_{20}Mn_{10}$	—	+1.2	—	+5

According to the Eq. (1), a negative ξ_2 value implies a negative temperature coefficient for the electrical conductivity at low temperatures, as it is observed in the experimental curve shown in Fig. 1. On the other hand, plugging the ξ_1 and ξ_2 values listed in Table I into Eq. (4) we obtain $([d^2 \ln \sigma(E)]/(dE^2))_{E=\mu} = -288 \pm 6$ (eV)$^{-2}$, indicating a negative curvature of the spectral conductivity function at the Fermi level. Making use of the Einstein's relation into Eqs. (3) and (4) we obtain

$$N'(E_F) = N(E_F)\left[2\xi_1 - \frac{D'(E_F)}{D(E_F)}\right], \quad (7)$$

$$N''(E_F) = 2N(E_F)\left[\xi_2 - \frac{1}{2}\frac{D''(E_F)}{D(E_F)} - \frac{N'(E_F)D'(E_F)}{N(E_F)D(E_F)}\right], \quad (8)$$

where the prime stands for the energy derivative. As a first approximation we will assume that the diffusivity term is energy independent.[35] In that case, the slope and curvature of the DOS at the Fermi level can be determined from the knowledge of $N(E_F)$ and the values of the phenomenological coefficients ξ_1 and ξ_2 through the expressions

$$\xi_1 = \frac{N'(E_F)}{2N(E_F)}, \quad \xi_2 = \frac{N''(E_F)}{2N(E_F)}. \quad (9)$$

The DOS value at the Fermi level has been determined from low temperature specific heat measurements to be $N(E_F) = 0.17$ states (eV)$^{-1}$/atom for the $Al_{73.6}Mn_{17.4}Si_9$ cubic approximant.[36] By plugging this value into Eq. (9), making use of the data listed in Table I, we obtain $N'(E_F) = 0.1 \pm 0.02$ states (eV)$^{-2}$/atom, and $N''(E_F) = -49 \pm 1$ states (eV)$^{-3}$/atom. The value of the ratio $|N''(E_F)|/N(E_F) = 290 \pm 20$ (eV)$^{-2}$ is 25% smaller than that reported for *i*-AlPdMn QCs [$N''(E_F)/N(E_F) = 384$ (eV)$^{-2}$] on the basis of NMR measurements.[37,38] Furthermore, the negative sign of the DOS second derivative indicates a local negative curvature, corresponding to a peak, rather than a dip, at the Fermi level position.

V. DERIVATION OF THE ELECTRONIC STRUCTURE MODEL PARAMETERS

To further substantiate this important result we will analyze the electronic structure of the approximant in more detail on the basis of the Landauro-Solbrig spectral conductivity model,[12–14]

$$\sigma(E) = \frac{\bar{B}}{\pi}\left\{\frac{\gamma_1}{(E-\delta_1)^2+\gamma_1^2} + \alpha\frac{\gamma_2}{(E-\delta_2)^2+\gamma_2^2}\right\}^{-1}. \quad (10)$$

This model satisfactorily describes the electronic structure of both QCs and AC close to the Fermi level in terms of a wide Lorentzian peak (related to the Hume-Rothery mechanism) plus a narrow Lorentzian peak (related to hybridization effects). This model includes six parameters, determining the Lorentzian's heights and widths, $1/(\pi\gamma_i)$, their positions with respect to the Fermi level, δ_i, and their relative weight in the overall structure, α. The parameter $\bar{B}$ is a scale factor measured in $(\Omega\,\mathrm{cm\,eV})^{-1}$ units. In the original approach these electronic model paramenters were firstly extracted by fitting Eq. (10) to the conductivity curve numerically obtained from *ab initio* calculations for approximants, and subsequently refined by comparing with experimental curves of suitable icosahedral phases.[12–14,39]

TABLE III. Electronic model parameters for the $Al_{73.6}Mn_{17.4}Si_9$ cubic approximant as derived from the knowledge of the phenomenological coefficients listed in Table I (left column). For the sake of comparison we list the model parameters for the $Al_{63}Cu_{25}Fe_{12}$ QC sample studied in Ref. 19 (right column).

$Al_{73.6}Mn_{17.4}Si_9$	$Al_{63}Cu_{25}Fe_{12}$
$\alpha = 0.21$	$\alpha = 1.07$
$\gamma_1 = +0.065$ eV	$\gamma_1 = +0.587$ eV
$\gamma_2 = +0.022$ eV	$\gamma_2 = +0.055$ eV
$\delta_1 = +0.023$ eV	$\delta_1 = -0.005$ eV
$\delta_2 = -0.029$ eV	$\delta_2 = -0.016$ eV

In our phenomenological approach, we will make use of experimental input from the very begining as provided by the set of phenomenological coefficients listed in Table I. From their knowledge we can derive the corresponding electronic model parameters following the algebraic procedure described in the Appendix. In this way, we obtain the electronic model parameters listed in Table III. Making use of the data listed in Table III, in Fig. 3 we compare the spectral conductivity functions corresponding to the $Al_{73.6}Mn_{17.4}Si_9$ cubic approximant considered in this work and the AlCuFe QC studied in Ref. 19. By inspecting this figure we see that the spectral conductivity of QC is both deeper and broader than that corresponding to the approximant phase, thus indicating a less effective Hume-Rothery mechanism for the AC. On the other hand, the presence of a well-defined spectral feature at about −0.03 eV may be indicative of hybridization effects likely related to bond formation in the approximant sample. Accordingly, our results support the view that short-range

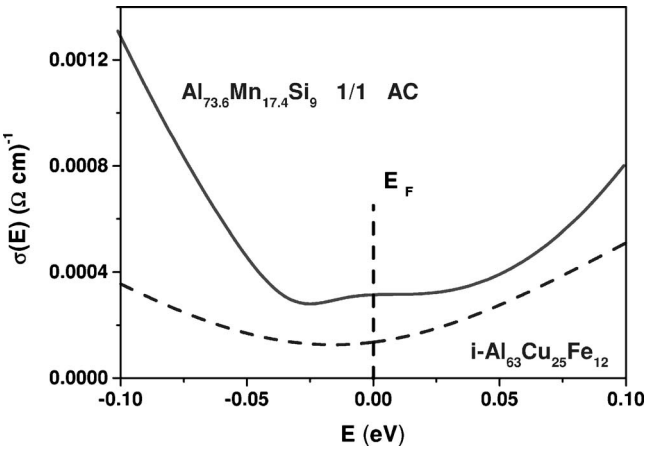

FIG. 3. Spectral conductivity function derived from the electronic model parameters listed in Table III for the $Al_{73.6}Mn_{17.4}Si_9$ cubic approximant (solid line) and an $Al_{63}Cu_{25}Fe_{12}$ icosahedral QC (dashed line).

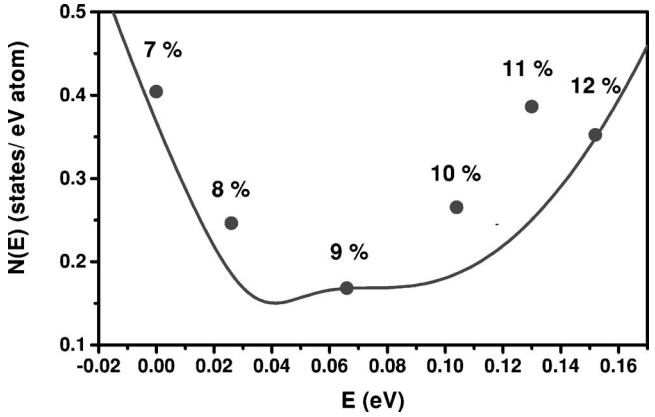

FIG. 4. Density of states derived from the measured electronic specific heat γ coefficients listed in Table IV for a complete series of $Al_{82.6-x}Mn_{17.4}Si_x$ 1/1-cubic approximants (solid circles). The silicon content of each sample is indicated in atomic percent. The solid line is the DOS curve derived from the spectral conductivity function plotted in Fig. 3 properly rescaled (more details in the main text).

chemical effects are playing a significant role in the stabilization of approximant phases.[40] Quite remarkably, the spectral conductivity function exhibits a reverse sign curvature at the Fermi level, as expected from the previous discussion about the physical meaning of the ξ_2 phenomenological coefficient sign, hence providing compelling evidence about the pinning of the Fermi level close to a fine structure in the DOS.

This interesting result can be experimentally checked by considering the DOS values at the Fermi level for a series of $Al_{82.6-x}Mn_{17.4}Si_x$ 1/1-cubic approximants. In fact, in Ref. 34 the $N(E)$ of $Al_{82.4-x}Re_{17.6}Si_x(7<x<12)$ 1/1-cubic approximants was systematically deduced from electronic specific heat measurements, obtaining a fairly good agreement with the $N(E)$ calculated by the linear muffin-tin orbital atomic-sphere approximation (LMTO-ASA) method with the well-refined structure parameters determined by the synchrotron Reitveld analysis. Furthermore, the measured thermoelectric power curves were properly accounted for in terms of this $N(E)$, hence providing additional support onto the reliability of the obtained DOS. In the light of these results, we concluded that substitution of Si atoms for Al atoms in amounts smaller than 5 at. % should not cause a large variation in the sample's electronic structure but a small increase in the electron concentration. A completely analogous result is expected for the $Al_{82.4-x}Mn_{17.6}Si_x(7<x<12)$ 1/1-cubic approximants considered in the present work, which can be obtained from the AlReSi approximant by simply replacing Re atoms with Mn ones (both located in the same column of the periodic table).

Accordingly, in Fig. 4, we plot the DOS values at the Fermi level as derived from the measured electronic specific heat coefficients listed in Table IV. Energies were calculated using the area of the trapezoid in the $N(E)$ curve and the electron concentration was determined from the sample composition. The solid line has been obtained by properly scaling the previously derived spectral conductivity function $\sigma(E)$ according to the expression

TABLE IV. Electronic specific heat γ coefficients and related DOS value at the Fermi level for a complete series of $Al_{82.6-x}Mn_{17.4}Si_x$ 1/1-cubic approximants. The listed DOS values include electron-phonon mass enhancement effects.

x	γ (mJ/mol K^2)	E (eV)	$N(E)$ (states/eV atom)
7	1.156	0	0.409
8	0.74	0.025	0.249
9	0.48	0.065	0.17
10	0.758	0.103	0.268
11	1.103	0.128	0.39
12	1.005	0.151	0.356

$$N(E) = \frac{N(E_F)}{\sigma(0)}\mu\sigma(E), \tag{11}$$

where $N(E_F)=0.17$ state/eV atom is the measured DOS value for the 9% Si sample, $\sigma(0)=318.4$ (Ω cm) is the electrical conductivity measured for this sample at $T=5$ K, and $\mu=10$ is a factor accounting for the charge carrier mobility. As we can see, most experimental points fit well to the rescaled electronic model curve when it is properly shifted in energies. Therefore, we can confidently conclude that at the Fermi level it is pinned near a DOS narrow peak rather than a dip in the considered sample. A similar pseudogap structure close to the Fermi level was reported by Zijlstra and Bose, where a shift in the Fermi level with increasing Si concentration in a nearly rigid pesudogap is also observable.[41] Unfortunately, the energy accuracy of the band structure calculations (50–100 meV) does not allow for a direct, quantitative comparison with our present results.

Finally, some words are in order regarding the range of applicability of our model approach. Certainly, experimental transport data for quasicrystalline samples have been analyzed by other authors in terms of alternative models, well beyond the description given in terms of Eq. (10).[42] Remarkably, nice fittings have been obtained in the context of two-band models by several groups.[24,43,44] Among them, only the model considered in Ref. 43 makes use of a smaller number of fitting parameters as compared to Eqs. (1) and (2) (this being a measure of a simpler description). Unfortunately, the values and signs of the resulting parameters are very difficult to interpret physically.[43] In other cases, the number of parameters is too large to perform suitable fitting, so that a number of reasonable assumptions was to be made concerninig the charge carriers density and relaxation time values.[44] To the best of our knowledge none of these models have been applied to study the transport properties of approximants to date in order to determine the influence of long-range versus short-range effects.

VI. CONCLUSIONS

In general, QCs and approximants are regarded as typical Hume-Rothery electron compounds mainly stabilized by the presence of a pseudogap at the Fermi level. Nonetheless, the contribution of hybridization effects involving sp-d electrons

should also play an important role, and even becomes the relevant stabilization mechanism in some instances.[45] Broadly speaking one can think of the Fermi surface-Brillouin zone interaction mechanism giving rise to the opening of the psudogap as mainly related to long-range order effects; meanwhile, hybridization effects giving rise to the possible formation of chemical bonds among certain atoms will be properly related to short-range effects. The results obtained in our phenomenological approach, based on a realistic $\sigma(E)$ model, lend support to the pseudogap induced phase stabilization, since a broad pseudogap has been found in the approximant phase. As expected, this pseudogap is not so deep as those observed in typical icosahedral phases. However, the Fermi level is located at a local peak of the DOS rather than at the minimum of the pseudogap, as occurs in most QCs. This facts suggest that the absence of a long-range quasiperiodic order in the AC precludes the Fermi surface-Brillouin zone mechanism of being so effective as it is in QCs. On the other hand, the characteristic temperature dependence observed in the thermopower curve is related to the presence of some fine spectral features in the $\sigma(E)$ curve which may be related to narrow features in the DOS. In particular, the presence of a narrow dip in the pseudogap, close to the Fermi level, has been found in the approximant phase. The possible existence of such features has been recently reported in some QCs by a number of high resolution, low temperature scanning tunneling studies.[46,47] In this sense, the possible presence of such features in approximant samples as well would be quite appealing.

ACKNOWLEDGMENTS

This work has been partially supported by the Ministerio de Educación y Ciencia through Project No. FIS2004-00067, the Consejería de Educación de la CAM and European Union FEDER through Project No. GR/MAT/0768/2004. One of the authors (T. T.) was financially supported by a MEXT Grant-in-Aid for Young Scientists No. (A) 17686054. E. M. acknowledges M. V. Hernández for a critical reading of the manuscript.

APPENDIX

The phenomenological coefficients ξ_j can be expressed in terms of the electronic model parameters as[16]

$$\xi_1 \equiv -\frac{\gamma_1\delta_1\varepsilon_2^4+\alpha\gamma_2\delta_2\varepsilon_1^4}{\varepsilon\varepsilon_1^4\varepsilon_2^4}, \tag{A1}$$

$$\xi_2 \equiv 4\xi_1^2+\frac{\gamma_1\epsilon_2^6(\varepsilon_1^2-4\delta_1^2)+\alpha\gamma_2\epsilon_1^6(\varepsilon_2^2-4\delta_2^2)}{\varepsilon\varepsilon_1^6\varepsilon_2^6}, \tag{A2}$$

$$\xi_3 \equiv \frac{42}{5}\frac{\alpha\gamma_1\gamma_2\delta}{\varepsilon^3\varepsilon_1^4\varepsilon_2^4}[\varepsilon(\varepsilon_2^2-\varepsilon_1^2)-2\delta m_1], \tag{A3}$$

$$\xi_4 \equiv \frac{21}{5}\frac{\alpha\gamma_1\gamma_2}{\varepsilon^4\varepsilon_1^6\varepsilon_2^6}[4\delta^2\varepsilon\varepsilon_1^2\varepsilon_2^2(\gamma_1+\alpha\gamma_2)-(4\delta m_1-\varepsilon(\varepsilon_2^2-\varepsilon_1^2))^2], \tag{A4}$$

where

$$\varepsilon=\gamma_1\varepsilon_1^{-2}+\alpha\gamma_2\varepsilon_2^{-2}, \tag{A5}$$

$\varepsilon_i^2=\gamma_i^2+\delta_i^2$, $\delta\equiv\delta_1\varepsilon_1^{-2}-\delta_2\varepsilon_2^{-2}$, and $m_1=\gamma_1\delta_2+\alpha\delta_1\gamma_2$.

In order to determine the electronic model parameters from the knowledge of the phenomenological coefficients, we introduce the following variables:

$$x\equiv\gamma_1/\varepsilon_1^2,\quad y\equiv\gamma_2/\varepsilon_2^2,\quad z\equiv\delta_1/\varepsilon_1^2,\quad w\equiv\delta_2/\varepsilon_2^2, \tag{A6}$$

satisfying the relationships

$$\varepsilon_1^{-2}=x^2+z^2,\quad \varepsilon_2^{-2}=y^2+w^2 \tag{A7}$$

$$x/z=\gamma_1/\delta_1,\quad y/w=\gamma_2/\delta_2 \tag{A8}$$

so that the electronic model parameters can be expressed in terms of the new variables as

$$\gamma_1=\frac{x}{x^2+z^2},\quad \delta_1=\frac{z}{x^2+z^2},\quad \gamma_2=\frac{y}{y^2+w^2},\quad \delta_2=\frac{w}{y^2+w^2}. \tag{A9}$$

From the study of the electrical conductivity curve we previously obtained the relationship $\varepsilon=\pi\bar{B}/\sigma_0$.[16] The value of the scale factor $\bar{B}$ can be estimated from *ab initio* calculations and the residual conductivity can be determined from a fitting analysis of the experimental $\sigma(T)$ curve. Making use of the value $\bar{B}=10^6/580\ (\Omega\,\mathrm{cm\,eV})^{-1}$ (Ref. 48) and $\sigma_0=312.6\ (\Omega\,\mathrm{cm})^{-1}$ (cf. Table I) we get $\varepsilon=17.327\ (\mathrm{eV})^{-1}$. Thus, the value of ε is a known input, which according to Eqs. (A5) and (A6) can be expressed as

$$\varepsilon=x+\alpha y\Rightarrow\alpha=\frac{\varepsilon-x}{y}. \tag{A10}$$

Making use of Eq. (A6) into Eq. (A1) we have

$$A=xz+\alpha yw\Rightarrow w=\frac{A-xz}{\varepsilon-x}, \tag{A11}$$

where $A\equiv-\xi_1\varepsilon$. Analogously, making use of Eq. (A6) into Eq. (A2) we have

$$G=x^3+\alpha y^3-3(xz^2+\alpha yw^2), \tag{A12}$$

where $G\equiv(\xi_2-4\xi_1^2)\varepsilon$. By properly combining Eqs. (A10)–(A12) we obtain

$$y^2=\frac{(G-x^3)(\varepsilon-x)+3xz(\eta-A)+3A^2}{(\varepsilon-x)^2}, \tag{A13}$$

where we have introduced the auxiliary variable

$$\eta\equiv\varepsilon z-A. \tag{A14}$$

Making use of Eq. (A6) into Eq. (A3), taking into account Eq. (A11), we have

$$C = x\eta[\varepsilon(x^2 - y^2 + z^2 - w^2) - 2(z - w)(\varepsilon(z + w) - A)], \tag{A15}$$

where $C \equiv 5\xi_3\varepsilon^3/42$. Making use of Eqs. (A11) and (A13) we can rewrite Eq. (A15) in the form

$$C(\varepsilon - x)^2 = -x\eta[(\varepsilon + x)\eta^2 + (\varepsilon - x)F], \tag{A16}$$

where $F \equiv 3A^2 - \varepsilon(\varepsilon x^2 - G)$.

Finally, making use of Eq. (A6) into Eq. (A4), taking into account Eq. (A15), we have

$$D = 4C(\eta + A) + x\frac{4\eta^2\varepsilon^2x^2(\varepsilon - x)^2 - 8C\eta(\varepsilon - x)^2 + 4x^2\eta^4 - [(\varepsilon + x)\eta^2 + (\varepsilon - x)F]^2}{(\varepsilon - x)^3}, \tag{A17}$$

where $D \equiv 5\xi_4\varepsilon^4/21$. By properly using Eq. (A16) and grouping terms we can express Eq. (A17) as a biquadratic polynomial in the variable η

$$\alpha(x)\eta^4 + \beta(x)\eta^2 + \gamma(x) = 0, \tag{A18}$$

where

$$\alpha(x) \equiv 15x^2 + 6\varepsilon x - 5\varepsilon^2, \tag{A19a}$$

$$\beta(x) \equiv 2(\varepsilon - x)[2\varepsilon^2x^2(\varepsilon - x) + (5x - 3\varepsilon)F], \tag{A19b}$$

$$\gamma(x) \equiv \frac{(\varepsilon - x)^2}{x}[(4AC - D)(\varepsilon - x) - xF^2]. \tag{A19c}$$

The solution of Eq. (A18) can be expressed as

$$\eta = \pm\sqrt{\frac{Q}{2\alpha}}, \tag{A20}$$

where $Q \equiv -\beta \pm \sqrt{\Delta}$, and $\Delta \equiv \beta^2 - 4\alpha\gamma$. By plugging Eq. (A20) into Eq. (A16) after some algebra we get the following algebraic equation in the variable x

$$\gamma x^4R^2 + 4\beta x^2SR + 16\alpha S^2 = 0, \tag{A21}$$

where we have introduced the auxiliary polynomials

$$P(x) \equiv 2\alpha(\varepsilon - x)F - \beta(\varepsilon + x),$$

$$R(x) \equiv P^2 - 2\beta(\varepsilon + x)P + \Delta(\varepsilon + x)^2,$$

$$S(x) \equiv \alpha^2C^2(\varepsilon - x)^4 + \gamma x^2(\varepsilon + x)P.$$

Equation (A21) can be numerically solved to obtain x. The corresponding values are then substituted into Eq. (A20) to obtain η, from which we derive z making use of Eq. (A14). From the knowledge of both x and z we derive the values of y and w by means of Eqs. (A13) and (A11), respectively. Finally, we will make use of Eqs. (A9) and (A10) to determine the original electronic model parameters.

[1] A. P. Tsai, in *Physical Properties of Quasicrystals*, edited by Z. M. Stadnik, Springer Series in Solid-State Physics Vol. 126 (Springer-Verlag, Berlin, 1998), p. 5.

[2] E. Maciá, J. M. Dubois, and P. A. Thiel, *Ullmann's Encyclopedia of Industrial Chemistry*, 6th ed., (Wiley-VCH, Winheim, 2002), 2002 January Release on CD-ROM.

[3] Ö. Rapp, in Ref. 1, p. 127.

[4] S. Roche, G. Trambly de Laissardière, and D. Mayou, J. Math. Phys. **38**, 1794 (1997).

[5] K. Kirihara and K. Kimura, Sci. Technol. Adv. Mater. **1**, 227 (2000); R. Tamura, A. Waseda, K. Kimura, and H. Ino, Phys. Rev. B **50**, 9640 (1994).

[6] T. Klein, C. Berger, D. Mayou, and F. Cyrot-Lackmann, Phys. Rev. Lett. **66**, 2907 (1991).

[7] A. Carlsson, Nature (London) **353**, 353 (1991).

[8] P. Häussler, R. Haberken, C. Madel, J. Barzola-Quiquia, and M. Lang, J. Alloys Compd. **342**, 228 (2002); P. Häussler, H. Nowak, and R. Haberken, Mater. Sci. Eng., A **294–296**, 283 (2000); C. Roth, G. Schwalbe, R. Knöfler, F. Zavaliche, O. Madel, R. Haberken, and P. Häussler, J. Non-Cryst. Solids **252**, 869 (1999).

[9] R. Tamura, T. Asao, M. Tamura, and S. Takeuchi, Mater. Res. Soc. Symp. Proc. **643**, K13.3.1 (2001); R. Tamura, T. Asao, and S. Takeuchi, Mater. Trans., JIM **42**, 928 (2001).

[10] H. Sato, T. Takeuchi, and U. Mizutani, Phys. Rev. B **64**, 094207 (2001); T. Takeuchi, T. Onogi, E. Banno, and U. Mizutani, Mater. Trans., JIM **42**, 933 (2001).

[11] K. Kirihara, T. Nagata, K. Kimura, K. Kato, M. Takata, E. Nishibori, and M. Sakata, Phys. Rev. B **68**, 014205 (2003).

[12] H. Solbrig and C. V. Landauro, Physica B **292**, 47 (2000); C. V. Landauro and H. Solbrig, Mater. Sci. Eng., A **294–296**, 600 (2000).

[13] C. V. Landauro and H. Solbrig, Physica B **301**, 267 (2001).
[14] C. V. Landauro, Ph.D. thesis, Technische Universität Chemnitz, 2002.
[15] E. Maciá, Appl. Phys. Lett. **81**, 88 (2002).
[16] C. V. Landauro, E. Maciá, and H. Solbrig, Phys. Rev. B **67**, 184206 (2003).
[17] E. Maciá, Phys. Rev. B **66**, 174203 (2002).
[18] E. Maciá, J. Appl. Phys. **93**, 1014 (2003).
[19] E. Maciá, Phys. Rev. B **69**, 132201 (2004).
[20] T. Takeuchi, T. Otagiri, H. Sakagami, T. Kondo, and U. Mizutani, *Proceedings MRS 2003*, 805, 105 (2004).
[21] T. Takeuchi, T. Onogi, T. Otagiri, U. Mizutani, H. Sato, K. Kato, and T. Kamiyama, Phys. Rev. B **68**, 184203 (2003).
[22] The upturn of the conductivity at low temperatures may be associated to the presence of Kondo-like effects due to the magnetic momoments of some Mn atoms, as discussed by J. J. Préjean, C. Berger, A. Sulpice, and Y. Calvayrac, Phys. Rev. B **65**, 140203(R) (2002).
[23] T. Klein, H. Rakoto, C. Berger, G. Fourcaudot, and F. Cyrot-Lackmann, Phys. Rev. B **45**, 2046 (1992).
[24] R. Haberken, G. Fritsch, and M. Härting, Appl. Phys. A **57**, 431 (1993).
[25] B. D. Biggs, S. J. Poon, and N. R. Munirathnam, Phys. Rev. Lett. **65**, 2700 (1990).
[26] F. S. Pierce, S. J. Poon, and B. D. Biggs, Phys. Rev. Lett. **70**, 3919 (1993).
[27] B. D. Biggs, Y. Li, and S. J. Poon, Phys. Rev. B **43**, 8747 (1991).
[28] F. S. Pierce, P. A. Bancel, B. D. Biggs, Q. Guo, and S. J. Poon, Phys. Rev. B **47**, 5670 (1993).
[29] A. Bilušic, D. Pavuna, and A. Smontara, Vacuum **61**, 345 (2001); A. Bilušic, A. Smontara, J. C. Lasjaunias, J. Ivkov, and Y. Calvayrac, Mater. Sci. Eng., A **294–296**, 711 (2000).
[30] The low temperature range of application depends on the intensity of weak localization effects in the considered sample.
[31] D. K. C. MacDonald, *Principles of Thermoelectricity* (John Wiley & Sons, Inc, New York, 1962), p. 71.
[32] T. Otagiri, T. Kondo, T. Takeuchi, and U. Mizutani, *AIWQ3 Proceedings*, 2004.
[33] F. Cyrot-Lackmann, Mater. Sci. Eng., A **294–296**, 611 (2000); F. Cyrot-Lackmann, in *New Horizons in Quasicrystals: Research and Applications*, edited by A. I. Goldman, D. J. Sordelet, P. A. Thiel, and J. M. Dubois (World Scientific, Singapore, 1997).
[34] T. Takeuchi, T. Otagiri, H. Sakagami, T. Kondo, U. Mizutani, and H. Sato, Phys. Rev. B **70**, 144202 (2004).
[35] Within the Bloch-Boltzamnn treatment this is equivalent to the assumption of energy independent group velocity and mean free path, as it was discussed in Ref. 34.
[36] This figure includes the electron-phonon mass renormalization correction estimated to be of about 20% in the considered sample.
[37] J. Dolinšek, M. Klanjšek, T. Apih, A. Smontara, J. C. Lasjaunias, J. M. Dubois, and S. J. Poon, Phys. Rev. B **62**, 8862 (2000); **66**, 189901(E) (2002). The values $N''(E_F)/N(E_F)=490$ (eV)$^{-2}$ for *i*-AlCuFe and $N''(E_F)/N(E_F)=2300$ (eV)$^{-2}$ for *i*-AlPdRe samples were also reported in this work.
[38] The value $N''(E_F)/N(E_F)\simeq 500$ (eV)$^{-2}$ was derived from a NMR study of *i*-AlCuRu samples as reported by E. A. Hill, T. C. Chang, Y. Wu, S. J. Poon, F. S. Pierce, and Z. M. Stadnik, Phys. Rev. B **49**, 8615 (1994).
[39] The spectral conductivity function can be also obtained by fitting the the Kubo-Greenwood formulas for the $\sigma(T)$, $S(T)$, and $R_H(T)$ transport coefficients over a broad temperature range as reported by P. Häussler, R. Haberken, C. Madel, J. Barzola-Quiquia, and M. Lang, J. Alloys Compd. **342**, 228 (2002).
[40] R. Asahi, H. Sato, T. Takeuchi, and U. Mizutani, Phys. Rev. B **71**, 165103 (2005).
[41] E. S. Zijlstra and S. K. Bose, Phys. Rev. B **67**, 224204 (2003).
[42] R. Haberken, G. Fritsch, and M. Härting, Appl. Phys. A **57**, 431 (1993).
[43] F. Giroud, T. Grenet, C. Berger, P. Lindqvist, C. Gignoux, and G. Fourcaudot, Czech. J. Phys. **46–S6**, 2709 (1996).
[44] T. Nagata, K. Kirihara, and K. Kimura, J. Appl. Phys. **49**, 6560 (2003).
[45] Y. Ishii and T. Fujiwara, Phys. Rev. Lett. **87**, 206408 (2001).
[46] O. Gröning, R. Widmer, P. Ruffieux, and P. Gröning (unpublished); T. Okada, T. Ekino, Y. Yokoyama, T. Takasaki, Y. Watanabe and S. Nanao (unpublished).
[47] R. Escudero, J. C. Lasjaunias, Y. Calvayrac, and M. Boudard, J. Phys.: Condens. Matter **11**, 383 (1999); R. Escudero (unpublished).
[48] H. Solbrig and C. V. Landauro, in *Quasicrystals Structure and Physical Properties*, edited by H. R. Trebin (Wiley-VCH, Weinheim, 2003), p. 254.